HIFAN 1621

Fast six-channel pyrometer for warm-dense-matter experiments with intense heavy-ion beams

P. A. Ni*
Lawrence Berkeley National Laboratory, University of California, Berkeley, California, USA
M. I. Kulish, V. Mintsev, D. N. Nikolaev, and V. Ya. Ternovoi
Institute of Problems of Chemical Physics, Chernogolovka, Russia
D. H. H. Hoffmann and S. Udrea
Institut fˇur Kernphysik, Technische Universit¨at Darmstadt, Darmstadt, Germany
A. Hug, N. A. Tahir, and D. Varentsov
Gesellschaft fˇur Schwerionenforschung mbH, Darmstadt, Germany

Accelerator Fusion Research Division
Ernest Orlando Lawrence Berkeley National Laboratory
University of California
Berkeley, California 94720

April 21, 2008

Fast six-channel pyrometer for warm-dense-matter experiments with intense heavy-ion beams

P. A. Ni*

Lawrence Berkeley National Laboratory, University of California, Berkeley, California, USA

M. I. Kulish, V. Mintsev, D. N. Nikolaev, and V. Ya. Ternovoi

Institute of Problems of Chemical Physics, Chernogolovka, Russia

D. H. H. Hoffmann and S. Udrea

Institut für Kernphysik, Technische Universität Darmstadt, Darmstadt, Germany

A. Hug, N. A. Tahir, and D. Varentsov

Gesellschaft für Schwerionenforschung mbH, Darmstadt, Germany

(Dated: April 21, 2008)

This paper describes a fast multi-channel radiation pyrometer that was developed for warm-dense-matter experiments with intense heavy ion beams at Gesellschaft für Schwerionenforschung mbH (GSI). The pyrometer is capable of measuring of brightness temperatures from 2000 K to 50000 K, at 6 wavelengths in visible and near-infrared parts of spectrum, with 5 nanosecond temporal resolution and several micrometers spatial resolution. The pyrometer's spectral discrimination technique is based on interference filters, which act as filters and mirrors to allow for simultaneous spectral discrimination of the same ray at multiple wavelengths.

PACS numbers:

I. INTRODUCTION

A study of the fundamental properties of warm-dense-matter (WDM) is an important subject as it has wide applications to various branches of basic and applied sciences. Experimental study of equation-of-state of WDM is of considerable interest to fundamental research of thermodynamic and hydrodynamic behavior of dense plasmas. This study will enable one to probe the validity of existing theories on stellar formation and evolution, compressibility of inertial fusion targets and existing models for strongly coupled high density plasmas [1–4].

The heavy ion synchrotron SIS-18 at GSI is a unique facility worldwide that delivers intense beams of highly energetic heavy ions. Using these heavy ion beams, it is possible to heat macroscopic volumes of matter to extreme conditions of temperature and pressure with fairly uniform physical conditions [1, 5, 6].

Recently, a series of WDM physics experiments with heavy ion beams have been carried out at the HHT (high temperature) experimental area of the plasma physics group at GSI [7–11]. In these experiments, metallic targets of macroscopic volumes were heated by intense uranium ion beams uniformly and quasi-isochorically (FIG. 1), thereby generating high-density, high-entropy states. The heated target material was expanding isentropically, passing through physical states located in the region of the boiling curve, two-phase liquid-gas

*Formely at Institut für Kernphysik, Technische Universität Darmstadt, Germany.

and the critical point. The heating beam intensity was $4.4 \cdot 10^9$ ^{238}U^{74+} ions with a particle energy of 350 AMeV. Ions were delivered in a single 120 ns bunch (FWHM), resulting in an estimated several kJ/g energy deposition in lead [5, 6]. The thermodynamic properties, i.e. temperature, pressure, expansion velocity and electrical conductivity, of the target were measured during the heating as well as the expansion phases [8–10].
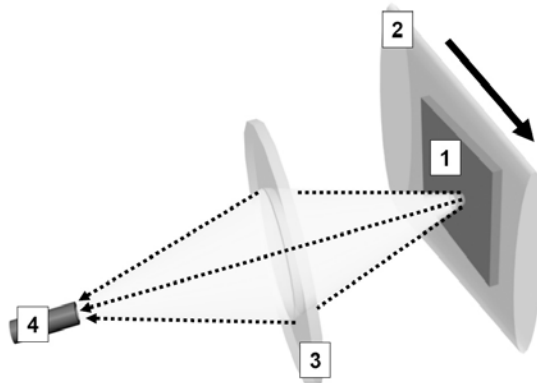

FIG. 1: Schematic layout of experiment: 1 — target sample, 2 — focused ion beam with elliptical profile, 3 — light collection optics capturing sample's thermal radiation, 4 — optical fiber connected to pyrometer.

This paper focuses on the six-channel pyrometer developed by scientists from GSI, TU-Darmstadt and IPCP. A pyrometer is a non-contact thermometer, which measures the temperature of an optically thick radiation layer, based on its emitted thermal radiation, while no distur-

bance of the existing temperature field occurs.

The developed instrument measures brightness temperatures at six wavelengths with 5 ns temporal resolution and 400 μm spatial resolution. The brightness temperatures are obtained from analysis of the Planck radiation in visible and near-infrared spectral regions [12, 13]. In addition, the absolute radiation emission recorded by the pyrometer at multiple wavelengths gives the possibility of application of various models of spectral emissivity. In some cases this leads to a more precise estimation of the physical temperature of the target [14–16].

In the performed WDM experiments, samples of various target materials including copper, aluminum, tungsten, tantalum, sapphire and uranium dioxide, were pulse heated by intense heavy ion beams and temperatures varying from 2000 K to 10000 K were measured. Different materials showed different hydrodynamic behavior clearly seen in the pyrometric records.

II. PYROMETER

The temporal resolution of the pyrometer suitable for the present experiments with heavy ion beams at GSI is dictated by the 120 ns heating beam duration and therefore must be on a nanosecond scale. A broad working range from 2000 K to 50000 K is also required since it is desirable to track temperature evolution during all phases of the experiment, which include pulsed heating with the ion beam and consequent cooling due to the free expansion into vacuum.

A. Light collection system

Efficient coupling of light into a pyrometer plays an important role and becomes more critical in experiments with lower temperatures ($\approx$ 2000 K). For WDM experiments at GSI, we have designed a collection optics system (condenser) which is compact enough to fit in the target vacuum chamber and at the same time relatively efficient, free from chromatic aberrations, having several micrometers spatial resolution and finally, matching the 0.22 numerical aperture (NA) of a fused silica, multi-mode fiber used for light coupling into the pyrometer.

The thermal radiation is analyzed in the spectral region from 500 nm to 1500 nm. Any condenser built from glass lenses and used in such a broad wavelength range will have chromatic abberations. This would effectively lead to wavelength dependence of the probing spot size and could be a critical issue in experiments with non-homogenous temperature distribution.

In order to exclude chromatic abberations, two different designs of light collection optics based on spherical and off-axis parabolic mirrors were implemented with the principal working scheme explained in FIG. 2 and FIG. 3.

In both designs, the sample is placed at the focus of the mirror producing a quasi collimated beam, which is
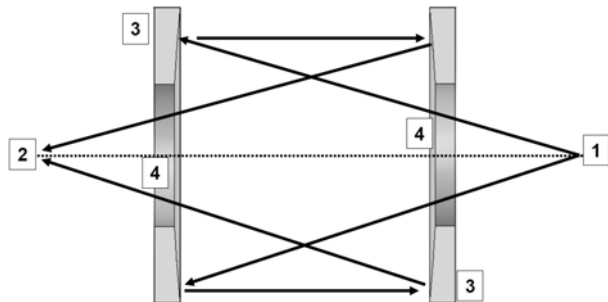

FIG. 2: Working scheme of spherical-mirror-based light collection optics (not to scale), thick lines — show propagation of light in the system: 1 — position of sample, 2 — position of optical fiber, 3 — spherical mirrors, 4 — central through bore.
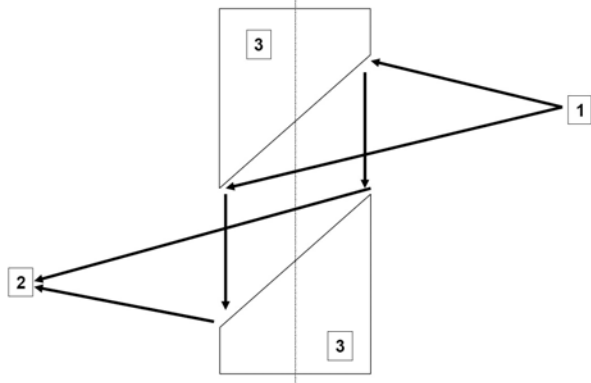

FIG. 3: Working scheme of parabolic-mirror-based light collection optics (not to scale), thick lines — show propagation of light in the system: 1 — position of sample, 2 — position of optical fiber, 3 — parabolic off-axis mirrors.

then focused on a fiber array using an identical second mirror. This arrangement produces a quasi 1:1 imaging of the target's surface.

The spherical mirrors (200 mm focal length, 80 mm diameter, central through bore 40 mm in diameter, protected silver coating, corrected for coma and spherical abberations) are a custom product manufactured by Laser Components GmbH after in-house sketches, while the parabolic mirrors (101 mm focal length, 50 mm diameter, silver coated) are a standard product of Janos Tech Inc.

The parabolic mirror condenser has a higher collection efficiency, however more difficult to align and has remarkable coma of probing areas with diameter greater than $\approx$ 0.5 mm. The spherical mirror system is less efficient but almost free from geometrical abberations and more suitable for probing of larger areas.

The fiber array consists of three 100 m long fibers (400μm core, laboratory-grade, fused-silica, low-OH, multi-mode, NA=0.22) with fiber cores placed on one line oriented horizontally. It allows for simultaneous application of multiple instruments, e.g. pyrometer and

spectrometers. Due to the 1:1 imaging of the optics, the probing area is equal to the diameter of the fiber core. In our experiments, we found 400 μm suitable both in terms of signal level and homogeneity of a sample's temperature distribution.

For positioning and fine adjustment, the entire optical assembly is mounted on a motorized table that can be moved along the XYZ axes with 1 μm precision. The setup is placed inside the vacuum chamber and can be controlled remotely.
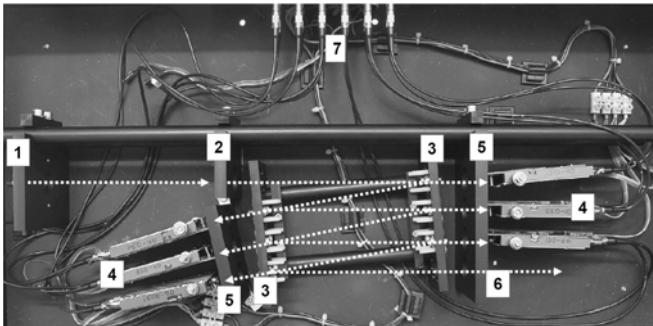
B. Spectral analyzer

FIG. 4: Photograph and principal working scheme of the spectral analyzer, with the dashed lines showing propagation of light within instrument: 1 — SMA-905 fiber coupling and 11 mm lens, 2 — collimating f=40 mm lens, 3 — array of interference filters (6 total), 4 — photo detectors (6 total), 5 — final focusing f=18 mm lenses (6 total), 6 — red diode laser, 7 — outputs to digitizers.

The collected thermal light is coupled to the spectral analyzer (see FIG. 4) via an SMA-905 fiber connector and discriminated at six wavelengths (channels). Two coated achromatic lenses (f=11 mm and f=40 mm) collimate the light into a quasi-parallel beam, which then undergoes successive reflections from six band pass interference filters. The mechanism of spectral resolution is based on the designed property of an interference filter being transparent for a narrow band of spectrum and acting as a mirror for the rest. The average peak transmission of filters varies from 30% to 70%, depending on the center wavelength.

The wavelength selection is chosen to include the peak of the Planck curve, which shifts from near-infrared to visible during a temperature change from 2000 K to 10000 K (range expected in present experiments). The filters are centered at 550 nm, 750 nm, 900 nm, 1100 nm, 1300 nm and 1500 nm, having width of 40 nm, 40 nm, 40 nm, 25 nm, 25 nm and 20 nm respectively. All filters are 1 inch in diameter and were purchased from the Andover Corporation.

The mounting sequence of filters within the spectrometer was chosen to provide optimal signal levels at all channels simultaneously, taking into account the sensitiv-

ity of detectors and spectral intensity of the calibration source (see section III).

Interference filters are designed to work at the normal incidence, while in our arrangement the angle is ≈ 5 degress. The changes in transmission due to non-normal incidence were investigated using a laboratory spectrometer. The observed difference turned out to be less than 1% shift of center wavelengths towards shorter wavelengths, which is small enough in comparison to the bandwidth of the filters.

The employed method of spectral discrimination is similar to the one proposed in [17] and has distinct advantages in terms of speed and efficiency, over conventional approaches, which include 45-degree beam splitters, time-multiplexed radiance onto a single detector using rotating filters, scanning spectrometer, etc.[12]. The utilized approach gives the possibility of simultaneous analysis of the very same beam at several wavelengths resulting in higher probing rates and no polarization dependance. Moreover, relatively low losses at each reflection allow for a higher number of channels.

At the final stage, the filtered light is focused by a f=18 mm aspherical lens to the detector consisting of a PIN photodiode connected to a custom transimpendence current amplifier. With the given parameters of collimation and focusing optics of the spectral analyzer, the final spot size is smaller than area of the detector. For fine positioning, the detector is mounted on a custom lockable kinematic stage. The fixation of the optics is stable and usually requires a single adjustment of optical components.

Two types of low-level dark-current photodiodes with 5 ns rise-time and 1 mm active are diameter are used: for channels from 550 nm to 900 nm, Si-diodes (Hamamatsu S7836-01), and for channels from 1100 nm to 1500 nm, InGaAs-diodes (Hamamatsu G8376-05). All detectors are run in a biased, linear regime with the flat amplification gain from DC to 0.7 GHz and the transimpedance gain of 75 kV/A. A conventional laboratory power supply provides 12 V DC.

A red diode laser is installed in the next free slot of the filter array and its position is adjusted so that its optical path is reverse to the propagation path of coupled light. The purpose of this laser is a quick check of the alignment of the filters in the array by measuring the laser power at the fiber input and comparing it with the value obtained during an optimal alignment of all filters.

The pyrometer is mounted in a chassis with a fiber and electrical inputs at the outer panels. The modular design allows for swapping and addition of various filters and detectors and can be upgraded to a higher number of channels.

C. Data acquisition hardware

Signal output of the pyrometer is recorded by a 24-channel, 8-bit digitizer (Acqiris DC271, 1 GHz band-

width, 4 Gs/s) into a 50 Ω load with DC coupling with all inputs of the digitizer being synchronized to a picosecond. The acquisition is triggered using a TTL signal coming from the accelerator and tied to the arrival of the ion beam at the target.

The digitizer is controlled remotely from a PC over the standard telecommunication optical fibers by means of specially written LabView code. This code incorporates basic features of a conventional oscilloscope and also allows for direct saving of data on a hard drive.

III. CALIBRATION

The pyrometer is calibrated [12, 13] with a tungsten ribbon lamp of the 'Pharaoh type', Osram W17/G powered by an ultra-stable DC power supply. The absolute radiation spectrum (2400 K at 650 nm) of a marked spot at the lamp's filament from 400 nm to 1600 nm (1 nm step) is provided by the manufacturer with 3% accuracy (NIST traceable).

The continuous radiation of the lamp is modulated at 1 kHz by a mechanical chopper (removed during experiments) installed right after the fiber input to the spectral analyzer. For minimizing the noise of the calibration signal the voltage values have been obtained from averaging over approximately 1000 acquisitions. Calibration is carried out with the very same components (condenser, vacuum feed-through, optical fiber, etc.) as in the experiments, and already includes optical transmission of all components. During the calibration and data processing, transmissions of the interference filter have been represented as Gaussian curves with FWHM corresponding to the documented width of the filters.

Typical calibration voltages start from 10 mV for the shorter wavelength channels, and reach 200 mV for the near infrared channels. The typical saturation voltage of the detector into a 50 Ω load is ≈1.9 V with the noise level at ≈ 0.02 V RMS. These numbers give rough estimations of lower and upper bounds of detectable black body temperatures determined by the noise level and the saturation voltage. For example, for the 550 nm channel, the detectable temperature range of a black body object is from 2400 K to 5000 K, while for the 1500 nm, it is from 1900 K to 9000 K. Higher temperatures can be measured by using an attenuation filter of a know transmission. The usage of an attenuator will also shift the lower temperature bond towards higher values.

Note that, because the emissivity of an optically thick body in thermal equilibrium is normally less than one, the detectable physical temperature is generally higher than the black body temperature [12].

IV. EXPERIMENTAL RESULTS

We demonstrate an experimental record of a tungsten target. In this experiment a free standing tungsten
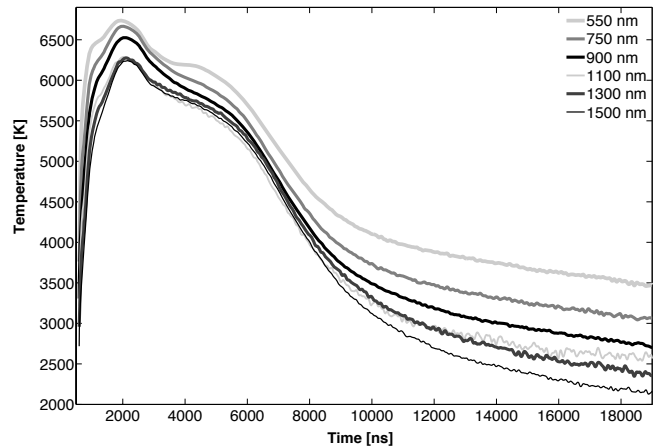

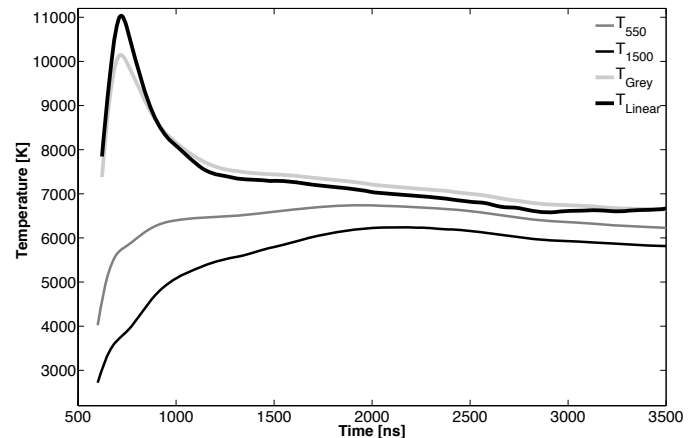FIG. 5: Brightness temperatures of ion beam heated tungsten foil (see details in text).

FIG. 6: Fitted temperatures obtained from the assumptions of grey or linear behavior of emissivity and brightness temperatures at 550 nm and 1500 nm.

foil, 100 μm thick, was pulse heated by an intense, focused ion beam and eventually expanded hydrodynamically into vacuum (see FIG. 1). The U^{74+} beam was, $4 \cdot 10^9$ particles/bunch, 120 ns FWHM, had an elliptical profile (width ≈ 100 μm) and irradiated the entire sample.

The pyrometer was probing a side of the sample (spot size 400 μm) and was aimed at the quasi-homogenous region of the Bragg energy deposition curve (ion range in tungsten is ≈ 2 mm). Brightness temperatures measured in this experiment are plotted in FIG. 5.

In order to determine the physical temperature of the sample in the experiment, knowledge of both brightness temperature and spectral emissivity is required [12, 13]. When emissivity in an experiment is not known, a way to approach the real value of temperature is to assume a
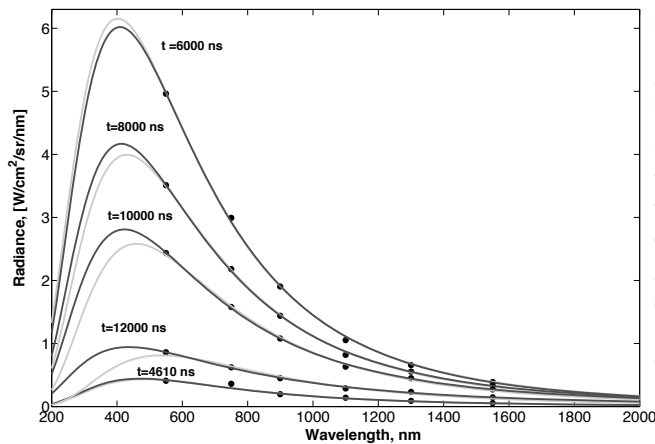
FIG. 7: Least-square fitting of experimental points (black circles) to radiation models with grey (grey) and linear (dark grey) behavior of emissivity at different moments of time.

plausible model [15, 16].

The employed pyrometer simultaneously measures the absolute radiation at multiple wavelengths, which gives an opportunity to apply various models of emissivity to experimental data at every point in time and to extract a temperature value from a non-linear least square fit [16].

Normally, the qualitative behavior of the emissivity in solid and cold liquid states is influenced both by surface conditions and optical constants of matter. In hot dense liquid and gaseous states, emissivity is governed mainly by the optical constants of the material which are related to electrical conductivity of the medium, and once the conductivity is known, optical constants can be obtained straightforwardly [18, 19].

The simplest and practical model of emissivity is based on the classical theory of conductivity proposed by Paul Drude in 1890 [20]. It can be shown that there exists a wide range of wavelengths extending from the visible region up to the near-infra-red region over which the emissivity of a solid and liquid metal to a good approximation, is constant (grey body) [20, 21].

This approximation is widely applied to liquid metals in metallurgy, where a disordered state washes out much of the band structure and the contribution of the specific conductive band is simplified [12, 22]. The grey body model is also valid in the case of several highly reflective solid metals like polished aluminium and silver [12] and also seems to be applicable in the the density region around 1 g/cm^3. As it was shown in [22], at this density value the electronic structure is simple enough to be de-

scribed by the Drude approximation. Such states appear, for example, during the release of a shocked metal.

Taking the above considerations into account, two empirical models of emissivity were applied in this work. The first one is the grey body approach as it is specifically justified for liquid and release states of WDM matter. The second model assumes a linear law of emissivity, which can be treated as a modified grey model with a linear term added. The linear model incorporates black and grey body cases and is a good approximation for some solid metals, e.g. tungsten [13].

In FIG. 6, we show results of data processing for the two models with brightness temperatures at 550 nm and 1500 nm also plotted for a comparison. FIG. 7 shows the actual fitting of these two models of radiation into experimental points at various moments of time.

The temperature values demonstrated in these plots are only an estimation of reality and an attempt to reduce the effect of the unknown emissivity. However, their physical sense, in general, is debatable, and therefore should be considered only as a reference and as a supplement to the primary pyrometer output — brightness temperatures.

V. SUMMARY

A fast multichannel pyrometer has been designed and successfully commissioned in the recent WDM physics experiments with heavy ion beams. The pyrometer is a primary diagnostic tool in the present and future high-energy-density physics experiments at GSI. A modification will be required, when the Facility for Antiproton and Ion Research (FAIR), the coming upgrade of GSI, will be operational, where higher and faster heating rates are expected. The instrument is designed such that an upgrade towards higher temperatures and higher speed can be carried out rather easily; components satisfying future regimes are available now. The new experimental data, developed diagnostics and experience gained from this work are also of great importance for planning future WDM physics experiments at FAIR [3, 5, 23].

VI. ACKNOWLEDGMENTS

[1] D.H.H. Hoffmann, et.al., Nucl. Instrum. and Meth. A 577, 8-13 (2007).
[2] B. G. Logan, F.M. Bieniosek, C.M. Celata, et.al., Nucl.

Instrum. and Meth. A 577, Issues 1-2, 1 (2007), Pages 1-7
[3] W. F Henning, Nucl. Instr. and Meth. B 214 (2004) 211.
[4] N. A. Tahir et al., Phys. Rev. Lett. 95, 035001 (2005).

[5] N. A. Tahir, et.al., Nucl. Instrum. and Meth. A 577, 238 - 249 (2007).

[6] N. A. Tahir, et.al., Nucl. Instr. Meth. A544, (2005)16-26.

[7] D.H.H. Hoffmann, et.al., Laser Part. Beams 23 (2005) 47.

[8] D. Varentsov, V.Ya. Ternovoi, et.al., Nucl. Instrum. and Meth. A 577, 262 - 266 (2007).

[9] M. Kulish, et al., GSI Report, no. GSI-2006-02, GSI-Darmstadt, (2006), p.12.

[10] S. Udrea, et.al., Nucl. Instrum. and Meth. A 577, 257-261 (2007).

[11] F. Becker, A. Hug, P. Forck, et.al., Laser and Particle Beams, Volume 24, Issue 04, pp 541-551 (2006)

[12] L. Michalski, K. Eckersdorf, J. Kucharski, J.McGhee, Temperature Measurement Second Edition, 2001, John Wiley & Sons, Inc.

[13] D. P. Dewitt, Therory and practice of radiation thermometry, John Wiley & Sons, Inc., (1998).

[14] J. L. Gardner, T. P. Jones and M. R. Davies, Appl. Opt. 13, 459(1981).

[15] M. A. Pellerin, B. K. Tsai, D. P. DeWitt, and G. J. Dall, in Temperature, Its Measurement and Control in Science and Industry, American Institute of Physics, Vol. 6, Part 2 (1992), p. 871.

[16] B. Coates. High Temperatures-High pressures, 20 pp 433-441(1988).

[17] J. L. Gardner, T. P. Jones, W.G. Sainty, Appl. Opt. 21, 1259(1982).

[18] Classical Electrodynamics by J.D. Jackson.

[19] E. Hagen und H. Rubens, Annalen der Physik, 4, 11 (1903).

[20] P. Drude, Annalen der Physik 14, 936 (1904).

[21] D. J. Price, 1949 Proc. Phys. Soc. A 62 278-283.

[22] P.Celliers and A. Ng, Phys. Rev. Lett., 90, 17.

[23] D.H.H. Hoffmann, et.al., Laser Part. Beams 23, 47-53 (2005).